Roe-inspired stem cell microcapsules for inflammatory bowel disease treatment

Guopu Chen[a,1], Fengyuan Wang[b,1], Min Nie[a], Hui Zhang[c], Han Zhang[c], and Yuanjin Zhao[a,c,d,2]

[a]Department of Rheumatology and Immunology, Institute of Translational Medicine, The Affiliated Drum Tower Hospital of Nanjing University Medical School, Nanjing 210002, China; [b]Department of Dermatology, Zhongda Hospital, Southeast University, Nanjing 210009, China; [c]State Key Laboratory of Bioelectronics, School of Biological Science and Medical Engineering, Southeast University, Nanjing 210096, China; and [d]Chemistry and Biomedicine Innovation Center, Nanjing University, Nanjing 210023, China

Edited by David A. Weitz, Harvard University, Cambridge, MA, and approved September 12, 2021 (received for review July 9, 2021)

Mesenchymal stem cells (MSCs), which exert regulatory effects on various immune cells, have been a promising therapy for inflammatory bowel disease treatment. However, their therapeutic effects are limited by lack of nutritional supply, immune system attack, and low accumulation on the target site. Here, inspired by the natural incubation mechanism of roe, we present immune-isolating, wet-adhesive, and nutrient-rich microcapsules for therapeutic MSCs encapsulation. The adhesive shells were fabricated by ionic cross-linking of alginate and visible curing of epsilon-poly-L-lysine-graft-methacrylamide and dopamine methacrylamide, which encapsulated the liquid core of the MSCs and roe proteins. Due to the core-shell construction of the resultant microcapsules, the MSCs might escape from attack of the immune system while still maintaining immunomodulating functions. In addition, the roe proteins encapsulated in the core phase offered sufficient nutrient supply for MSCs' survival and proliferation. Furthermore, after intraperitoneal transplantation, the wet-adhesive radicals on the shell surface could immobilize the MSCs-encapsulating microcapsules onto the bowel. Based on these features, practical values of the roe-inspired microcapsules with MSCs encapsulation were demonstrated by applying them to treat dextran sulfate sodium (DSS)–induced colitis through increasing residence time, regulating immune imbalance, and relieving disease progression. We believe that the proposed roe-inspired microcapsules with MSCs encapsulation are potential for clinical application.

microfluidics | microcapsule | mesenchymal stem cell | hydrogel | inflammatory bowel disease

Inflammatory bowel disease (IBD), including Crohn's disease (CD) and ulcerative colitis, incorporates a spectrum of chronic inflammatory diseases of the gastrointestinal tract, and its overall occurrence is increasing globally (1–4). Various drugs and diverse strategies have been developed for IBD treatment targeting different molecules and cells related to the pathogenesis of IBD, including immunomodulators, amino salicylates, and corticosteroids (5–8). However, their therapeutic effects are unsatisfactory with high recurrence rates even after long-term maintenance, and the patients may suffer from a persistent inflammation and life of poor quality (9–11). As alternative strategies to treat IBD, cellular therapeutics such as mesenchymal stem cells (MSCs) have been employed as an attractive candidate (12–16). These MSCs can exert regulatory effects on various immunocytes, including dendritic cells, natural killer cells, macrophages, and lymphocytes, to modulate the immune imbalance of IBD (17–22). Although they have had many successes, the injected MSCs will be immediately identified and eliminated by the immune cells; thus, the clinical therapeutic effect of MSCs is greatly challenged by short survival time (23–27). In addition, it is challenging to manage MSCs onto the target site to guarantee sufficient therapeutic effects (28, 29). Therefore, new MSC therapy strategies with increased fitness, persistence, and targeting are still anticipated.

In this study, inspired by the natural incubation mechanism of roe, we proposed a microfluidic MSC microcapsule with embryo-like structure and wet-adhesive property for IBD treatment, as schemed in Fig. 1. Microfluidic generated microcapsules have been proposed as a bioengineering technology to encapsulate stem cells in a semipermeable immune-isolating membrane for therapeutic applications (30–36). However, due to lacking design of the shell, most of the current microcapsules can be administered with difficulty at the target site to maintain effective therapeutic effects (37, 38). In addition, it is challenging to supply enough nutrients for encapsulated MSCs proliferation in the microcapsules. In contrast, some natural roes, such as those ovulated by the Asian carp, have been evolving a special physiological structure to maintain species continuation. Generally, the core-shell structures of these roes can protect the cores from the external hostile environment, and the adhesive substance in their shell surface can immobilize them onto underwater objects that are not easily taken away by the current to increase their survival rate. More importantly, these roes are rich in nutrient to support themselves developing into fish (39, 40). However, biomimetic construction of such roe-like multifunctional microcapsules for MSCs encapsulation has never been investigated.

Here, we employed an electrostatically driven coaxial microfluidics to fabricate immune-isolating, wet-adhesive, and nutrient-rich microcapsules for therapeutic MSCs encapsulation. The electrostatically driven microfluidics can encapsulate the MSCs in oil-free water phases and maintain the bioactivity

Significance

We present roe-inspired microcapsules for therapeutic mesenchymal stem cells (MSCs) encapsulation with immune-isolating, wet-adhesive, and nutrient-rich capabilities. Due to the core-shell structure, the encapsulated MSCs could escape from the immune system and maintain immunomodulating functions. Furthermore, the roe proteins encapsulated with MSCs in the core phase provided adequate nutritional supply. By adding epsilon-poly-L-lysine-graft-methacrylamide and dopamine methacrylamide in the shell phase, the microcapsules might securely attach to the surface of the bowels. The encapsulated MSCs could relieve inflammatory bowel disease through modulating macrophage polarization. Based on these features, the roe-inspired microcapsules have great research value in clinical application.

Author contributions: Y.Z. designed research; G.C., F.W., and M.N. performed research; G.C. contributed new reagents/analytic tools; G.C. and M.N. analyzed data; and G.C., F.W., Hui Zhang, and Han Zhang wrote the paper.

The authors declare no competing interest.

This article is a PNAS Direct Submission.

[1]G.C. and F.W. contributed equally to this work.

[2]To whom correspondence may be addressed. Email: yjzhao@seu.edu.cn.

This article contains supporting information online at http://www.pnas.org/lookup/suppl/doi:10.1073/pnas.2112704118/-/DCSupplemental.

Published October 22, 2021.

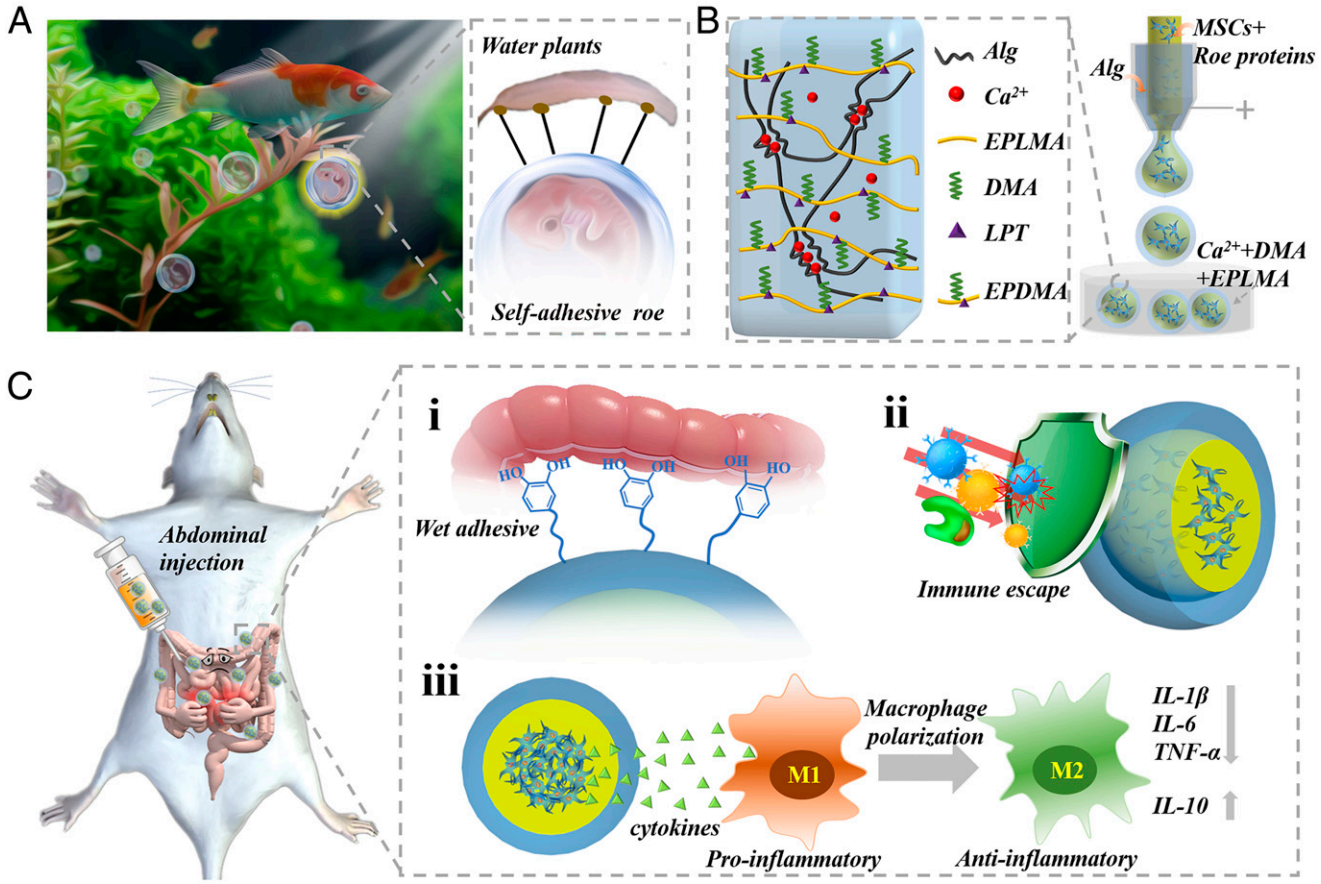

Fig. 1. Schematics of application of the bioinspired, immune-isolating, wet-adhesive, and nutrient-rich microcapsules with MSC encapsulation for IBD treatment. (*A*) Self-adhesive roes survive in nature and can adhere onto the surface of wet plants. (*B*) Fabrication process of the wet-adhesive and nutrient-rich microcapsules with MSC encapsulation. The shell was formed by a double network of Alg hydrogel and EPDMA hydrogel. (*C*) Application of the microcapsules in IBD treatment through abdominal injection: (*i*) wet adhesion, (*ii*) immune escape, and (*iii*) immunoregulation mechanism of the microcapsule.

of the cells. The adhesive shells of the microcapsules were formed by quick ionic cross-linking alginate (Alg) and visible curing of epsilon-poly-L-lysine-graft-methacrylamide (EPLMA) and dopamine methacrylamide (DMA) in the outer layers of the microfluidic droplets. Thus, the liquid cores of the MSCs and roe proteins were encapsulated inside the shells. We have demonstrated that the resultant core-shell–structured microcapsules could isolate the MSCs from immune cells and the roe proteins in the core phase provided sufficient nutrients for survival and proliferation of MSCs. In addition, the wet-adhesive substances EPLMA/DMA (EPDMA) in the shell could immobilize microcapsules onto the surfaces of bowels after intraperitoneal administration. It was found that the roe-inspired microcapsules could increase cellular half-life, regulate immune disorder, and relieve disease progression in colitis mouse. These results indicated that the resultant roe-inspired microcapsules were valuable in IBD treatment and promising for various disease treatments.

Results

According to the experiment, the DMA was derived from the condensation of methacrylic anhydride with dopamine (*SI Appendix*, Figs. S1*A* and S2), whereas the EPLMA was synthesized by covalently modifying epsilon-poly-L-lysine with methacrylic anhydride (*SI Appendix*, Figs. S1*B* and S3). Accuracy of the MSCs was identified through flow cytometric analysis, as the expression of human leukocyte antigen-DR (HLA-DR), CD14, CD19, and CD45 was less than 1%, while that of the CD73 and CD105 was more than 95% (*SI Appendix*, Fig. S4). The roe-inspired stem cell microcapsules (RSMs) were fabricated from an electrostatically driven coaxial microfluidics system. The inner phase, composed of the roe proteins and MSCs solution, was flowed inside the inner capillary tube, while the Alg solution was flowed along the outer tapered capillary tube as the outer phase. Due to the hydrodynamic focusing effect, the inner phase could be sheathed by the outer phase upon merging. Afterwards, the coflow was dispersed into mixed solution of $CaCl_2$ and EPLMA/DMA in the gelling pool. The rapid infusion of Ca^{2+} could immediately solidify the shell phase, while the visible light could cure the EPLMA/DMA, which was cross-linked by lithium phenyl-2,4,6-trimethylbenzoylphosphinate (LPT) (*SI Appendix*, Fig. S1*C*) to form a double network shell structure of the microcapsules. Meanwhile, the inner roe proteins and MSCs were kept liquid to form an embryo-like, core-shell structure (Fig. 2*A*). By dynamic regulation of the flow velocity, collecting distance and voltage, precise control of the size of the microcapsules, and ratio of the shell/core diameters could be achieved while keeping good monodisperse (*SI Appendix*, Figs. S5 and S6).

To evaluate the potential prospect and biomedical application value of the RSM, the biocompatibility of the microcapsule was first tested. For this purpose, 3T3 fibroblasts were employed to evaluate the biotoxicity of the simple microcapsules via the extraction method (*SI Appendix*, Fig. S7). The

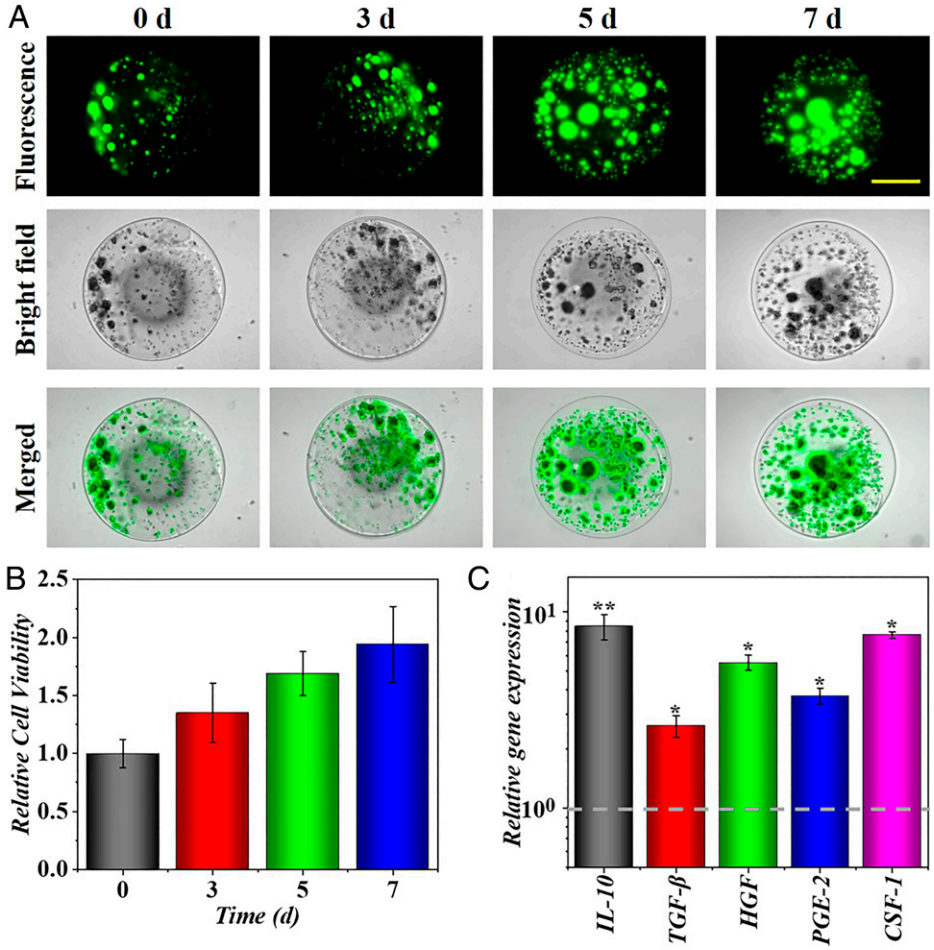

Fig. 2. Cell proliferation and immunomodulatory function of the RSMs. (*A*) Representative fluorescent images of the MSCs encapsulated in the roe-inspired microcapsules at days 0, 3, 5, and 7. (*B*) Quantitative analysis of the cell viability of MSCs in the roe-inspired microcapsules. (*C*) Functionalized gene expression of MSCs encapsulated in roe-inspired microcapsules normalized to conventional plate culture. (Scale bar in *A*, 100 μm.) $*P < 0.05$, $**P < 0.01$.

viability of cells dealt with different extraction concentrations kept over 90% after coincubation for 48 h compared with the blank control group. In addition, to effectively encapsulate MSCs, the biocompatibility of the core phase with different concentrations of roe proteins was evaluated. Within certain limits, the cell viability increased following the increased concentration of roe proteins. However, the cell viability decreased when the concentration of the roe proteins was over 15% (*SI Appendix*, Fig. S8). This result should be ascribed to the beneficial nutritional support of roe proteins on the MSCs, but it may induce hyperosmosis and low pH when the concentration is too high. Thus, 10% roe proteins were chosen as the core phase for the following experiments. Trypan Blue analysis was employed to evaluate membrane integrity of MSCs after encapsulation, and no significant effect of high voltage on encapsulated MSCs was observed compared to initial cells (*SI Appendix*, Fig. S9). In addition, the roe-bioinspired microcapsules allowed a rapid cell growth during the 7-d culture (Fig. 2 *A* and *B*) and kept high cell viability after 14-d culture (*SI Appendix*, Fig. S10). It was demonstrated that cell clusters could be formed with the extension of culture time due to the proliferating cells. The increased percentage of living MSCs in roe-like microcapsules revealed a good proliferation capability because of the biocompatible microenvironment provided by the microcapsules, which could offer nutrient support.

To investigate the potential effects of the RSM in IBD treatment, the production capacity of immunomodulatory proteins and cytokines was detected by using quantitative real-time PCR. As shown in Fig. 2*C*, a range of genes relevant to immunomodulatory factors could be expressed by the MSCs, such as IL-10, TGF-β, HGF, PGE-2, and CSF-1. Higher gene expressions could be achieved after RSM encapsulation, showing an enhanced immunomodulatory function. In addition, immobilization of RSMs onto the intestine surface could be beneficial to enhance therapeutic effects of the encapsulated MSCs; hence, the adhesive capacity of the RSM onto the surface of the intestine was tested. Based on the catechol group of the adhesive substance EPDMA in the shell, the adhesive energy of RSMs was significantly higher than RSMs with no adhesive substance addition (NARSMs) (*SI Appendix*, Fig. S11*A*), whose shells were composed of simple Alg hydrogel. The RSMs and NARSMs were then dyed red, and it was found that the RSMs could adhere tightly onto the surface of small intestine, cecum, and colon tissue at top, side, and bottom sites (Fig. 3 *A* and *B*). Furthermore, a constant number of RSMs and NARSMs dispersed in the phosphate-buffered saline (PBS) solution were employed to flow through the intestine surface. The RSM group was observed remaining on the intestine surface, while the NARSM group slipped away. Afterwards, simple PBS flow was used to simulate peritoneal fluid to flush the microcapsules on the intestine surface three times. The results showed that parts of the NARSMs were flushed away, while almost all RSMs immobilized at the original sites (Fig. 3 *C* and *D*). Statistical analysis of adhesion rate was evaluated by counting the

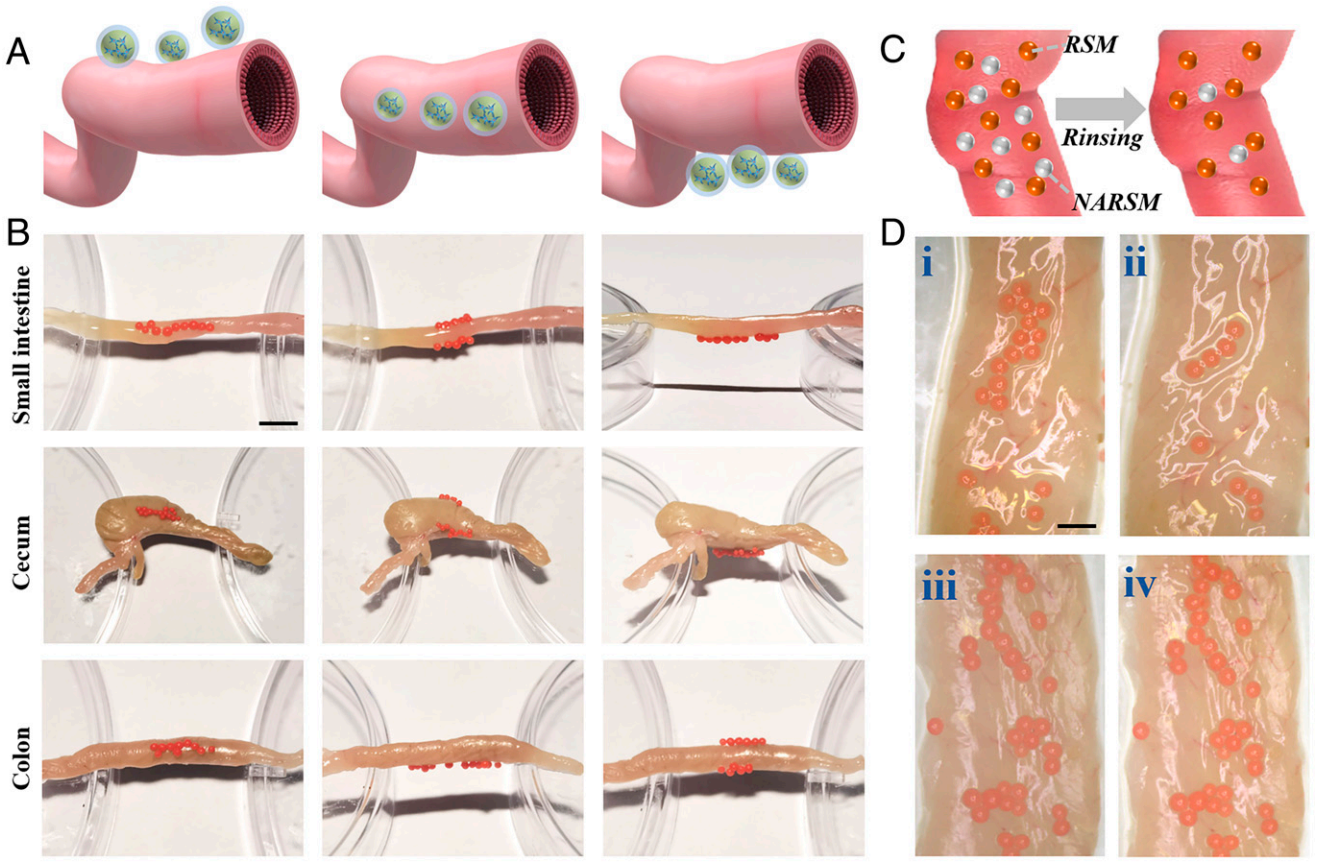

Fig. 3. Adhesion capacity tests of RSMs. (*A*) Schematics of the adhesion of RSMs to top, side, and bottom of the intestine. (*B*) Digital images of the RSMs adhering to the top, flank, and bottom of different segments of the intestine. (*C*) Schematics of wet-adhesion property test of the RSMs after rinsing. (*D*) Digital images of wet-adhesion property test of the microcapsules after the first flow of (*i*) simple microcapsules without adhesive substance, (*iii*) microcapsules with adhesive substance, and their corresponding digital images after three rinses (*ii*, *iv*). (Scale bar in *B*, 0.5 cm; scale bar in *C*, 1 mm.)

microcapsules left on the intestine surface. The adhesion rate of RSMs was about 80%, which was obviously higher than the NARSMs (*SI Appendix*, Fig. S11*B*), indicating satisfactory adhesion capacity of the RSMs.

Considering the application of intraperitoneal injection and large numbers of macrophages in the abdomen, the regulating effect of MSCs on macrophages was also evaluated to explore the immune regulation mechanism in disease treatment. The peritoneal macrophages were pretreated by lipopolysaccharide (LPS) and then cocultured with RSMs. The results showed that the activated macrophages expressed lower proinflammatory cytokines such as IL-1β, IL-6, and TNF-α and the higher anti-inflammatory cytokine IL-10 with the existence of RSMs (Fig. 4*A*). Furthermore, similar results could be observed in the cocultured supernatants (Fig. 4*B*). It was demonstrated that the RSMs could polarize proinflammatory peritoneal macrophages (M1 macrophages) into anti-inflammatory phenotype (M2 macrophages), relieving inflammatory response in the IBD. The proinflammatory cytokines IL-1β, IL-6, and TNF-α secreted by M1 macrophages led to the characteristic inflammatory response of IBD, while anti-inflammatory cytokine IL-10 secreted by M2 macrophages had a significant effect on suppressing immune response to relieve the symptoms of IBD. The residence time of MSCs in vivo greatly influences their therapeutic effects, as they are easily eliminated by the immune cells. Therefore, the persistence time of RSMs in vivo was evaluated. After intraperitoneal transplantation, the RSMs could adhere and immobilize firmly on the surface of bowel without transposition. The roe-inspired adhesive shell phase with catechol structure could adhere to the tissue through hydrogen bonds and improve the stabilization of the microcapsules. In addition, a firefly luciferase reporter was employed to transduce MSCs; afterwards, pure MSCs and MSCs encapsulated microcapsules were injected into the abdominal cavity respectively. The mice were imaged at 0 d, 3 d, and 5 d after transplantation (Fig. 4*C*). The pure MSCs were rapidly eliminated after injection, while encapsulation in the microcapsules significantly increased the residence time. The core-shell structure of microcapsules could protect MSCs from immune cells and provide abundant nutrients.

To evaluate the practical value of the RSM in IBD treatment, a dextran sulfate sodium (DSS)–induced colitis model was established. All the mice were divided into five groups that were the normal control group and DSS-induced colitis treated with PBS, microcapsule, MSCs, and RSM, respectively. Macroscopically, colon length is important to evaluate the therapeutic efficacy. Compared to the normal group, the colons in PBS- and microcapsule-treated groups were significantly shorter, indicating that the DSS-induced colitis model was successfully established. On the contrary, colitis mice who received treatment with RSM showed much less colon shortening (Fig. 5 *A* and *B*). In addition, the disease activity index (DAI) was evaluated, which was the summation of the consistency index, weight loss index, and fecal bleeding index. It was found that significantly reduced body weights and increased DAI could be observed in PBS- and microcapsule-treated groups, while the MSCs and RSM groups promoted body weight recovery and reduced DAI (Fig. 5 *C* and *D*). Furthermore, histological sections were examined. Increased

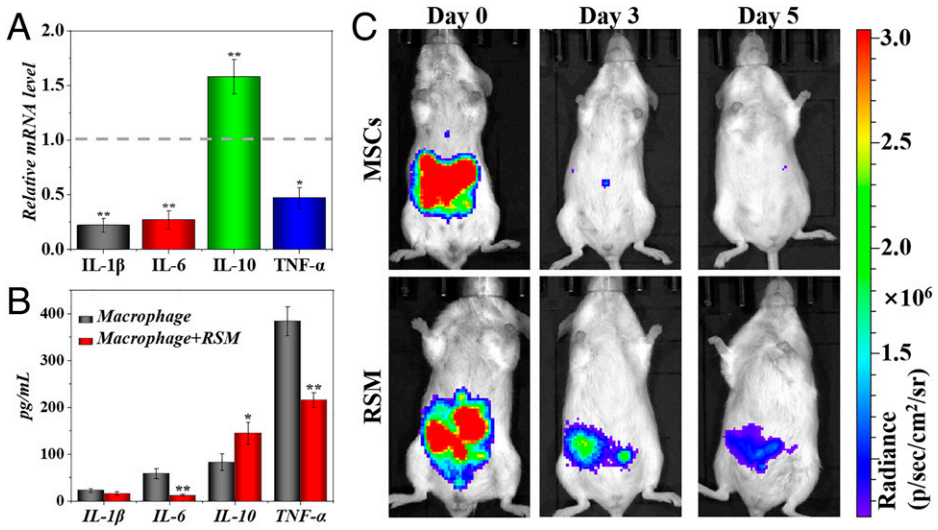

Fig. 4. Immune-modulating function and in vivo residence capability of RSMs. (*A*) Relative mRNA expression of IL-1β, IL-6, IL-10, and TNF-α expressed by macrophages cocultured with RSMs. (*B*) Protein expression levels of IL-1β, IL-6, IL-10, and TNF-α in the supernatant. (*C*) Residence time of the simple MSCs and RSM after intraperitoneal administration. $n = 6$ per group (*A*, *B*). $^{*}P < 0.05$, $^{**}P < 0.01$.

inflammatory infiltration, serious necrocytosis, damaged mucus membranes, and destroyed crypt structures could be observed in PBS- and microcapsule-treated colitis mice. However, RSM-treated mice exhibited a nearly normal pathological structure, indicating that RSM ameliorated the histopathologic damage induced by DSS (Fig. 5*F*).

To further investigate the biological mechanism of RSM in treating IBD, different inflammation-related mediators in bowel tissues were evaluated. Myeloperoxidase (MPO) indicates the degree of neutrophil infiltration in the inflammatory bowel and is closely related to the severity of IBD. MPO was obviously increased in PBS- and microcapsule-treated groups compared to that in the normal group and was significantly reduced in the MSCs and especially RSM groups (Fig. 5*E*). In addition, the levels of proinflammatory cytokines, including IL-6 and TNF-α, were obviously decreased, and the anti-inflammatory cytokine IL-10 increased in the RSM-treated group compared to those without RSM treatment (Fig. 6 *C*–*E*). Furthermore, the impact of RSMs on barrier function was tested. Immunofluorescence staining revealed that mice with colitis exhibited damaged epithelial tight junctions with reduced protein expressions of claudin and zona occludens 1 (ZO-1), while the RSM could reverse protein reduction to preserve the intestinal barrier (Fig. 6 *A* and *B*). These results demonstrated that the RSM was ideal for IBD treatment and have potential for more important applications in biomedical engineering.

Discussion

To conclude, we have developed roe-inspired microcapsules with MSCs encapsulation for IBD treatment by using a microfluidic electrospray. An electrostatically driven coaxial microfluidics system was used to fabricate the bioinspired microcapsules equipped with Alg and adhesive EPDMA shells to encapsulate the MSCs and roe proteins cores. After intraperitoneal administration, the adhesive shell of the resultant microcapsule could stick onto the surface of the bowels. In addition, the core-shell structure could protect the encapsulated MSCs from the immune system while maintaining the immune regulating capabilities. Furthermore, the encapsulated roe proteins in the core continuously offered nutrient supply for the survival and proliferation of MSCs. From the in vivo study, it was also shown that the roe-inspired microcapsules with MSCs encapsulation could perform well in treating DSS-induced colitis mice through increasing persistent time, regulating immune disorder, and relieving disease progression. These results demonstrated that the roe-inspired microcapsules with MSCs encapsulation were promising in treating IBD and valuable for various disease treatments.

Materials and Methods

Materials. Sodium Alg (low viscosity), *N*-hydroxysuccinimide (NHOSu), methacrylic anhydride (MA), N,*N*-dimethylformamide (DMF), epsilon-poly-L-lysine (EPL), (N,N′-dicyclohexylcarbodiimide (DCC), PBS, sodium bicarbonate, sodium tetraborate decahydrate, and dopamine hydrochloride were purchased from Aladdin. The ZO-1 and cludin antibodies and Cell Counting Kit-8 (CCK-8) were obtained from Abcam. The Dulbecco's Modified Eagle Medium: Nutrient Mixture F-12 (DMEM/F12), Trypsin–EDTA solution, and fetal bovine serum were obtained from Gibco. The sturgeon roe proteins were purchased from Xi'an Quanao Biotech Co., Ltd. All the antibodies were used according to the respective manufacturers' instructions.

Cells. The human umbilical cord–derived MSCs were obtained from Nanjing Taisheng Biological Technology Co., Ltd. Flow cytometric analysis was employed to identify the cell surface markers of MSCs, and the results showed that the expression of CD73 and CD105 was over 95%, while expression of CD14, CD19, CD45, and HLA-DR was less than 1%. The 3T3 fibroblasts were obtained from Wuhan Google Biotechnology Co., Ltd. The sequences of all the primers employed for qRT-PCR were listed in *SI Appendix*, Table S1.

Synthesis of EPLMA. NHOSu (0.465 g, 4.05 mmol) and MA (0.315 g, 3.67 mmol) were dispersed in 5 mL DMF. DCC (3.02 g, 0.755 mmol) was dispersed in 5 mL DMF and gradually added into the NHOSu/MA solution; afterward, the mixed solution was kept at 0 °C for 1.5 h and then stirred for 3 h at room temperature. EPL (10 g, 3.335 mmol) was dissolved in water/DMF (100 mL:50 mL) solution. The DCC solution was added to EPL solution after filtration and stirred together for 24 h. Afterward, the mixed solution was concentrated by rotary evaporator, precipitated in acetone, and filtered. The resultant product was dissolved in 100 mL deionized water and the undissolved powder removed through filtration. The solution was dialyzed in deionized water for 3 d, and powder was collected by vacuum freeze-drying.

Synthesis of DMA. Sodium bicarbonate (4 g, 47.6 mmol) and sodium tetraborate decahydrate (10 g, 26.2 mmol) were dispersed in 100 mL deionized water under mild heat. The solution was degassed with nitrogen gas for half an hour, followed by adding dopamine hydrochloride (5 g, 26.35 mmol). The mixture of 2.5 mL MA and 12 mL tetrahydrofuran was added to the dopamine solution. The mixed solution was stirred at room temperature for 18 h under nitrogen gas protection. Afterward, the solution was washed by ethyl acetate, acidified to acidic pH (less than 2), and extracted with ethyl acetate for three times.

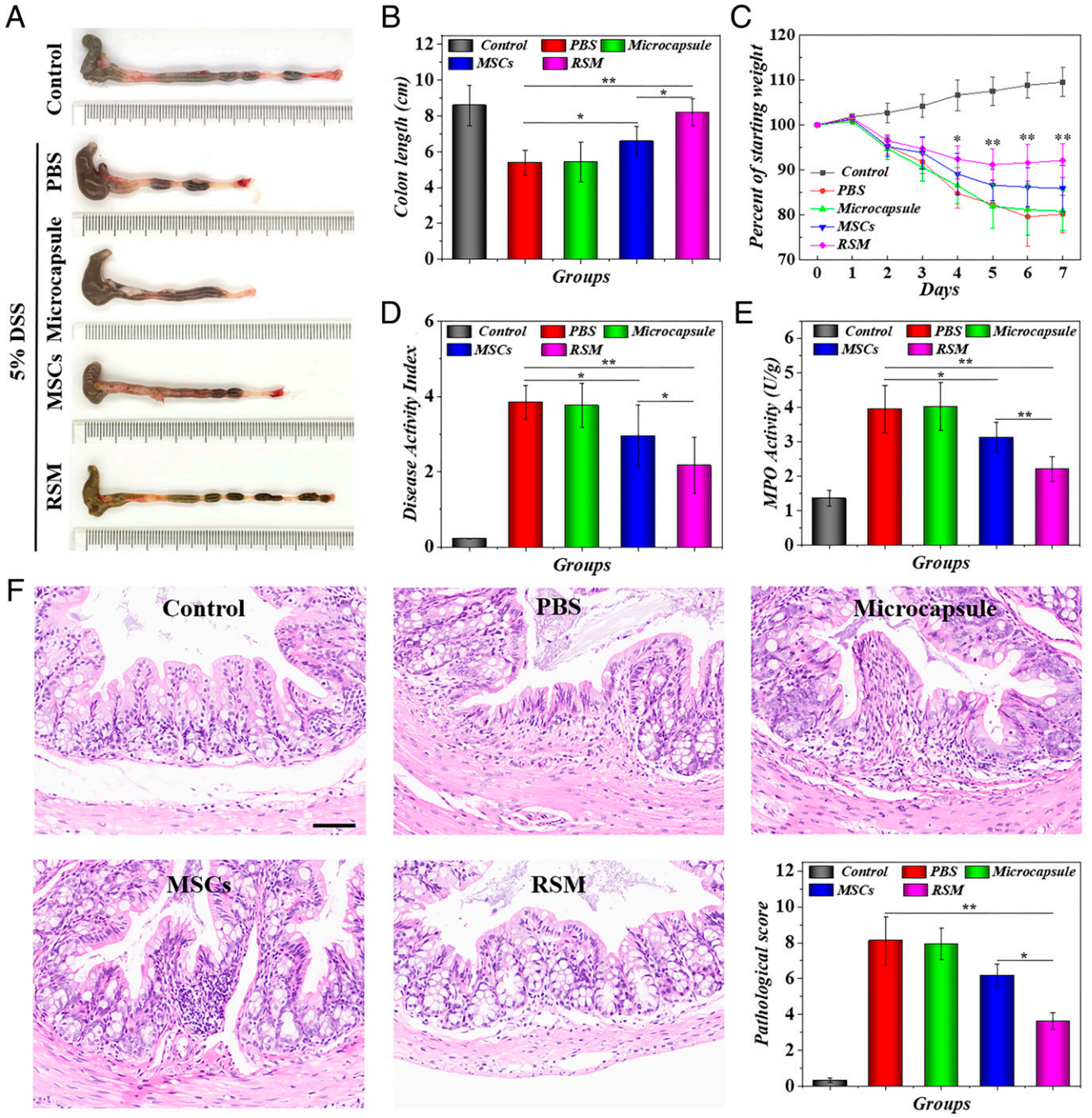

Fig. 5. The therapeutic efficacy of RSMs on DSS-induced colitis. (*A*) Colon appearance of normal control, and DSS-induced colitis treated with PBS, microcapsule, MSCs, and RSMs at day 7. (*B*) Quantitative analysis of colon length. (*C*) Body weight change within 7 d. (*D*) DAI and (*E*) MPO activity at day 7. (*F*) Hematoxylin and eosin staining and pathological scores of the colon tissues at day 7. $n = 6$ per group (*B–F*). (Scale bar in *F*, 100 μm.) $^{*}P < 0.05$, $^{**}P < 0.01$.

Microfluidic Device Design. Tapered capillaries and glass slides were used to fabricate the microfluidic device. The portable Bunsen burner was used to pull the inner capillary to form spindle tips, and the end of the outer capillary was drawn into a diameter of about 150 μm. Afterward, the inner capillary was coaxially placed into the outer tapered capillary and fixed by epoxy glue. An injection needle with notches was placed at the joint of the above fixed capillaries and fixed by epoxy glue.

Fabrication of the MSC Encapsulated Microcapsules. Before the experiment, the microfluidic device was autoclaved. A solution of 2% Alg was used to form the shell phase, while roe protein solution containing 1×10^6/mL MSCs and 2% carboxymethylcellulose (CMC) was used to form the core phase. The coflow broke into microdroplets under the electric field formed by a voltage power supply. The generated microdroplets were solidified in the gelling pool with 2% calcium chloride, 5% EPLMA and 5% DMA. After ionic cross-linking of Alg and calcium chloride, the microcapsules were transplanted into culture medium for visible light curing of EPLMA and DMA. The size of microcapsules could be controlled by adjusting voltage, collecting distance, flow rate of inner phase (F_{inner}), and flow rate of outer phase (F_{outer}). The microcapsules with or without MSCs encapsulated were photographed by microscopy (OLYMPUS IX71). Membrane integrity of MSCs prior to and after encapsulation was assessed by Trypan Blue exclusion method.

Biocompatibility of the Shell Phase. Extract solution method was employed to test biocompatibility of the shell phase, which was a kind of stand method that employed to evaluate biocompatibility of drugs or medical devices in the

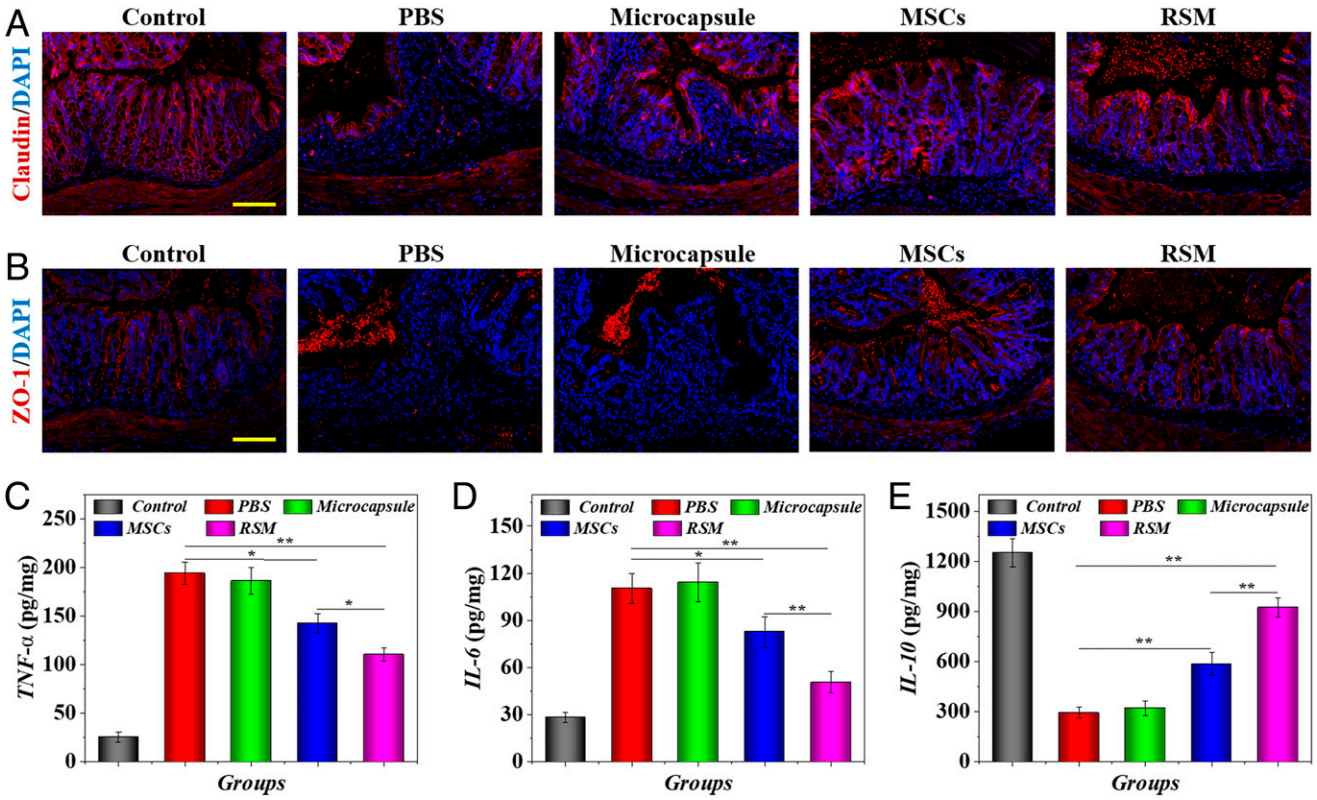

Fig. 6. Biological mechanism in RSMs treating colitis. (*A*) Representative immunostaining images of claudin (red) and DAPI (blue) in colon tissues. (*B*) Representative immunostaining images of ZO-1 (red) and DAPI (blue) in colon tissues. Protein levels of (*C*) cytokine TNF-α, (*D*) cytokine IL-6, and (*E*) cytokine IL-10 in colon tissues at 7 d from each group. $n = 6$ per group (*C*–*E*). (Scale bars in *A* and *B*, 100 μm.) $^{*}P < 0.05$, $^{**}P < 0.01$.

biomedical field. The shell hydrogels (72.5, 150, 300, and 600 mg, respectively) were added into each well and immersed in 1 mL culture medium for 24 h to obtain different extract solutions. The 3T3 fibroblasts (4,000 cells per well) were cultured in 96-well cell culture dishes for 24 h to achieve attachment before the experiment. Afterwards, the media was removed, and the cells were rinsed with PBS. The above extract solutions of different concentrations were added into each well and incubated with the cells for another 48 h. The CCK-8 assay was employed to measure the cell viability.

Biocompatibility of the Core Phase. The MSCs (4,000 cells per well) were cultured in 96-well culture dishes and cocultured with DMEM/F12 for 24 h. Afterwards, 5%, 10%, 15%, and 20% roe proteins were added, respectively, and incubated for another 24 h. The cell viability was measured by calcein staining and photographed by the fluorescent microscope.

MSC Proliferation in the Microcapsules. After cultured for different times, the proliferation of MSCs encapsulated in microcapsules was tested by using a blue fluorometric double-stranded DNA quantitation kit. Briefly, the MSCs encapsulated microcapsules were lysed in after two freeze–thaw cycles at −80 °C. Afterwards, the microcapsules were ground by a pestle to release cellular DNA and then centrifuged at 10,000 rpm for 15 min. After centrifugation, the liquid supernatants were collected and dyed with DNA conjugate. The DNA amount in each group was calculated based on a standard curve.

Adhesion Tests of the Microcapsules. The microcapsules employed in this test were dyed by red mineral dye. Microcapsules with EPLMA/DMA added were put onto the surface of small intestine, cecum, and colon tissue at the top, side, and bottom sites, and photo images were taken. Afterwards, 50 simple microcapsules without EPLMA/DMA added and microcapsules with EPLMA/DMA added were dispersed in PBS solution, respectively, and flowed through the colon surface. Simple PBS flow was employed to rinse the microcapsules on the colon surface three times. To calculate the adhesion rate, number of microcapsules remained on the colon surface was counted.

Isolation and Culture of LPS-Induced Peritoneal Macrophage. The balb/c mice received intraperitoneal injection of brewer thioglycolate medium (1 mL, 3%) once a day for 3 d. Afterwards, exudate cells in the abdomen were collected by 5mL RPMI medium 1640 through peritoneal lavage. Cells were transplanted in culture dish, and nonadherent ones were eliminated after 2 h incubation. Furthermore, the left adherent cells were cocultured with LPS for another 3 h and then cultured with RSM.

In Vivo Residence Time. MSCs were transfected with luciferase. Mice were equally divided into two groups, and received intraperitoneal injection with simple MSCs and MSCs encapsulated microcapsules respectively. D-luciferin was intraperitoneally injected to react with luciferase for imaging MSCs, and then luminescence images were photographed by the bioluminescence system (Caliper IVIS Lumina XR). Images were taken at 0, 3, and 5 d to assess the in vivo residence time of MSCs.

Acute DSS-Induced Colitis Treatment. Female 8- to 12-wk balb/c mice were obtained from Drum Tower Hospital. All animal experimental protocols were performed in accordance with the Guide for the Care and Use of Laboratory Animals and received approval from the Animal Investigation Ethics Committee of the Drum Tower Hospital. Mice received 5% DSS (40,000 kDa, Sigma) in the drinking water for 7 d to establish the DSS-induced colitis model. Afterwards, mice were divided into four groups randomly, which were treated with PBS, Microcapsule, MSCs, and RSM, respectively, for another 7 d. Weight was daily recorded and reported as the percentage of weight loss compared to the pretreatment weight. The severity of DSS colitis was assessed by the DAI. Mice have free access to feed and water during the experimental period.

Mice were fasted for 5 h at the end of the experiment and then anesthetized with 5% chloral hydrate and euthanized by cervical dislocation. The proximal colon tissues were excised and cut into two parts; one part was preserved in paraformaldehyde for further histology analysis, and the other part was preserved in liquid nitrogen. The colon tissues fixed with paraformaldehyde were then embedded in paraffin, and serial sections with thickness of 5 μm were obtained by microtome. The sections were stained with hematoxylin and eosin, ZO-1, and claudin for analysis by microscopy. Histologic score was determined in a blinded fashion by two investigators. The colon tissues preserved in liquid nitrogen were used to test the expression of MPO, TNF-α, IL-6, and IL-10.

Data Availability. All study data are included in the article and/or *SI Appendix*.

ENGINEERING

ACKNOWLEDGMENTS. This work was supported by the National Key Research and Development Program of China (Grant 2020YFA0908200), the National Natural Science Foundation of China (Grants 52073060 and 61927805), Jiangsu science and technology project (Grant BK20190353), and the Shenzhen Fundamental Research Program (Grant JCYJ201908131 52616459).

1. K. Parikh *et al.*, Colonic epithelial cell diversity in health and inflammatory bowel disease. *Nature* **567**, 49–55 (2019).
2. D. B. Graham, R. J. Xavier, Pathway paradigms revealed from the genetics of inflammatory bowel disease. *Nature* **578**, 527–539 (2020).
3. U. Jain *et al.*, *Debaryomyces* is enriched in Crohn's disease intestinal tissue and impairs healing in mice. *Science* **371**, 1154–1159 (2021).
4. S. C. Ng *et al.*, Worldwide incidence and prevalence of inflammatory bowel disease in the 21st century: A systematic review of population-based studies. *Lancet* **390**, 2769–2778 (2017).
5. S. Olafsson *et al.*, Somatic evolution in non-neoplastic IBD-affected colon. *Cell* **182**, 672–684.e11 (2020).
6. P. Gaffney, R. Gaffney, Pathophysiology of inflammatory bowel diseases. *N. Engl. J. Med.* **384**, 1377 (2021).
7. J. P. Gisbert, M. Chaparro, Predictors of primary response to biologic treatment [Anti-TNF, Vedolizumab, and Ustekinumab] in patients with inflammatory bowel disease: From basic science to clinical practice. *J. Crohn's Colitis* **14**, 694–709 (2020).
8. W. A. Goodman, I. P. Erkkila, T. T. Pizarro, Sex matters: Impact on pathogenesis, presentation and treatment of inflammatory bowel disease. *Nat. Rev. Gastroenterol. Hepatol.* **17**, 740–754 (2020).
9. A. Anderson *et al.*, The association between sustained poor quality of life and future opioid use in inflammatory bowel disease. *Inflamm. Bowel Dis.* **24**, 1380–1388 (2018).
10. D. J. Gracie, P. J. Hamlin, A. C. Ford, The influence of the brain-gut axis in inflammatory bowel disease and possible implications for treatment. *Lancet Gastroenterol. Hepatol.* **4**, 632–642 (2019).
11. L. Gonczi *et al.*, Perceived quality of care is associated with disease activity, quality of life, work productivity, and gender, but not disease phenotype: A prospective study in a high-volume IBD centre. *J. Crohn's Colitis* **13**, 1138–1147 (2019).
12. M. Carvello, A. Lightner, T. Yamamoto, P. G. Kotze, A. Spinelli, Mesenchymal stem cells for perianal Crohn's disease. *Cells* **8**, 764 (2019).
13. X. Cao *et al.*, IGF-1C hydrogel improves the therapeutic effects of MSCs on colitis in mice through PGE_2-mediated M2 macrophage polarization. *Theranostics* **10**, 7697–7709 (2020).
14. J. Z. H. Ko, S. Johnson, M. Dave, Efficacy and safety of mesenchymal stem/stromal cell therapy for inflammatory bowel diseases: An up-to-date systematic review. *Biomolecules* **11**, 82 (2021).
15. T. H. Shin *et al.*, TNF-α priming elicits robust immunomodulatory potential of human tonsil-derived mesenchymal stem cells to alleviate murine colitis. *Biomedicines* **8**, 561 (2020).
16. Y. Zhang *et al.*, Programmable and multifunctional DNA-based materials for biomedical applications. *Adv. Mater.* **30**, e1703658 (2018).
17. M. Nie *et al.*, Bio-inspired adhesive porous particles with human MSCs encapsulation for systemic lupus erythematosus treatment. *Bioact. Mater.* **6**, 84–90 (2020).
18. Y. Wei *et al.*, Chirality controls mesenchymal stem cell lineage diversification through mechanoresponses. *Adv. Mater.* **31**, e1900582 (2019).
19. C. Terraza-Aguirre *et al.*, Mechanisms behind the immunoregulatory dialogue between mesenchymal stem cells and Th17 cells. *Cells* **9**, 1660 (2020).
20. M. Lopez-Santalla, R. Hervas-Salcedo, M. Fernandez-Garcia, J. A. Bueren, M. I. Garin, Cell therapy with mesenchymal stem cells induces an innate immune memory response that attenuates experimental colitis in the long term. *J. Crohn's Colitis* **14**, 1424–1435 (2020).
21. L. Wu *et al.*, Hierarchical micro/nanofibrous membranes of sustained releasing VEGF for periosteal regeneration. *Biomaterials* **227**, 119555 (2020).
22. W. K. Wong, B. Yin, A. Rakhmatullina, J. Zhou, S. H. D. Wong, Engineering advanced dynamic biomaterials to optimize adoptive T-cell immunotherapy. *Eng. Regener.* **2**, 70–81 (2021).
23. F. Y. Wang, X. X. Zhang, G. P. Chen, Y. J. Zhao, Living bacterial microneedles for fungal infection treatment. *Research* **2020**, 2760594 (2020).
24. H. Zhang *et al.*, Immunotherapeutic silk inverse opal particles for post-surgical tumor treatment. *Sci. Bull. (Beijing)* **65**, 380–388 (2020).
25. S. Qi *et al.*, Cellular internalization-induced aggregation of porous silicon nanoparticles for ultrasound imaging and protein-mediated protection of stem cells. *Small* **15**, e1804332 (2019).
26. B. Dai *et al.*, Bioinspired janus textile with conical micropores for human body moisture and thermal management. *Adv. Mater.* **31**, e1904113 (2019).
27. G. L. Ying *et al.*, Aqueous two-phase emulsion bioink-enabled 3D bioprinting of porous hydrogels. *Adv. Mater.* **30**, e1805460 (2018).
28. Y. S. Zhang, A. Khademhosseini, Advances in engineering hydrogels. *Science* **356**, eaaf3627 (2017).
29. Q. Zhang, Y. Yang, L. Yildirimer, T. Xu, X. Zhao, Advanced technology-driven therapeutic interventions for prevention of tendon adhesion: Design, intrinsic and extrinsic factor considerations. *Acta Biomater.* **124**, 15–32 (2021).
30. J. Wang, C. M. Shao, Y. T. Wang, L. Y. Sun, Y. J. Zhao, Microfluidics for medical additive manufacturing. *Engineering* **6**, 1244–1257 (2020).
31. T. M. Choi *et al.*, Photonic microcapsules containing single-crystal colloidal arrays with optical anisotropy. *Adv. Mater.* **31**, e1900693 (2019).
32. X. Liu, W. Zheng, X. Jiang, Cell-based assays on microfluidics for drug screening. *ACS Sens.* **4**, 1465–1475 (2019).
33. L. Mou, B. Hu, J. Zhang, X. Jiang, A hinge-based aligner for fast, large-scale assembly of microfluidic chips. *Biomed. Microdevices* **21**, 69 (2019).
34. Y. R. Yu, J. H. Guo, B. Ma, D. G. Zhang, Y. J. Zhao, Liquid metal-integrated ultra-elastic conductive microfibers from microfluidics for wearable electronics. *Sci. Bull. (Beijing)* **65**, 1752–1759 (2020).
35. Y. Zhang *et al.*, Electrocoalescence of liquid marbles driven by embedded electrodes for triggering bioreactions. *Lab Chip* **19**, 3526–3534 (2019).
36. Y. Piao *et al.*, Biomedical applications of gelatin methacryloyl hydrogels. *Eng. Regener.* **2**, 47–56 (2021).
37. Y. Song *et al.*, Budding-like division of all-aqueous emulsion droplets modulated by networks of protein nanofibrils. *Nat. Commun.* **9**, 2110 (2018).
38. X. Feng *et al.*, Mechanical and antibacterial properties of tannic acid-encapsulated carboxymethyl chitosan/polyvinyl alcohol hydrogels. *Eng. Regener.* **2**, 57–62 (2021).
39. M. Pšenička, Rapid de-adhesion of northern pike *Esox lucius* eggs using sodium hypochlorite. *Fish Physiol. Biochem.* **44**, 1535–1539 (2018).
40. Y. S. Chang, F. L. Huang, Fibroin-like substance is a major component of the outer layer of fertilization envelope via which carp egg adheres to the substratum. *Mol. Reprod. Dev.* **62**, 397–406 (2002).